

# Synthesis and Optical Properties of Triphenylene-Based Dendritic Donor Perylene Diimide Acceptor Systems

Mahuya Bagui,<sup>†</sup> Tanmoy Dutta,<sup>†</sup> Sanjiban Chakraborty,<sup>†</sup> Joseph S. Melinger,<sup>‡</sup> Haizhen Zhong,<sup>§</sup> Andrew Keightley,<sup>||</sup> and Zhonghua Peng<sup>\*,†</sup>

<sup>†</sup>Department of Chemistry, University of Missouri-Kansas City, Kansas City, Missouri 64110, United States

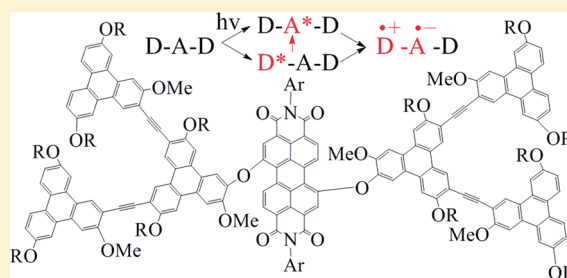
<sup>‡</sup>Naval Research Laboratory, Electronics Science and Technology Division, Washington, D.C. 20375, United States

<sup>§</sup>Department of Chemistry, University of Nebraska-Omaha, Omaha, Nebraska 68162, United States

<sup>||</sup>School of Biological Sciences, University of Missouri-Kansas City, Kansas City, Missouri 64110, United States

**S** Supporting Information

**ABSTRACT:** A donor–acceptor charge transfer system based on two discotic mesogens has been synthesized. The donor is either a triphenylene (POG0) or a triphenylene-based conjugated dendron (POG1), while the acceptor is a perylene diimide (PDI) core. The donors are covalently linked to the bay positions of the PDI core through an ether linkage. In chloroform, due to the short donor–acceptor distance and the matching frontier orbital levels, photoinduced charge transfer from either the donor excitation or the acceptor excitation are both thermodynamically and kinetically favored, resulting in efficient quenching of both donor and acceptor fluorescence. In a less polar solvent, hexane, while charge transfer is still the dominant mechanism for decay of the excited electronic state of POG1, photoinduced charge transfer is no longer energetically favorable for POG0 when the acceptor PDI core is excited, making the PDI core of POG0 weakly fluorescent in chloroform but strongly so in hexane. In solid film, POG0 is highly aggregated through both PDI–PDI and triphenylene–triphenylene homotopic stacking. POG1, on the other hand, aggregates through triphenylene dendrons with limited PDI–PDI core stacking, presumably due to the steric hindrance caused by bulky triphenylene moieties which block the access to the PDI core. The efficient photoinduced charge transfer, coupled with the homotopic stacking that forms separated electron-transporting PDI-stacked columns and hole transporting triphenylene-stacked columns, suggests that the reported donor–acceptor systems based on dual-discotic mesogens are potentially new efficient photovoltaic materials.



## INTRODUCTION

One of the most elegant systems in nature is its photosynthetic reaction center, where a photoinduced electron transfer process (PET) converts harvested solar energy into chemical energy.<sup>1</sup> An understanding of energy and electron transfer processes in a donor–acceptor (D-A) architecture is essential to the development of artificial photosynthetic systems.<sup>2</sup> D-A systems also play an important role in the construction of molecular electronic devices.<sup>3</sup> In this context, dendrimers are an important class of macromolecules whose convergent architecture naturally suggests them as an ideal framework to build D-A systems.<sup>4</sup> Dendrimers possess numerous peripheral end groups that all converge to a single core. By careful engineering of a large number of donor branches around a single acceptor and the optimization of donor to acceptor distances, an efficient light harvesting dendrimer can be realized.<sup>5</sup> Indeed, a large number of light harvesting dendrimers, including both conjugated<sup>6–8</sup> and nonconjugated<sup>9</sup> skeletons, have been developed and their excitation energy transfer dynamics have been thoroughly explored.<sup>10</sup>

Among various organic acceptors, perylene diimides (PDIs) are perhaps the most extensively studied systems, not only due to

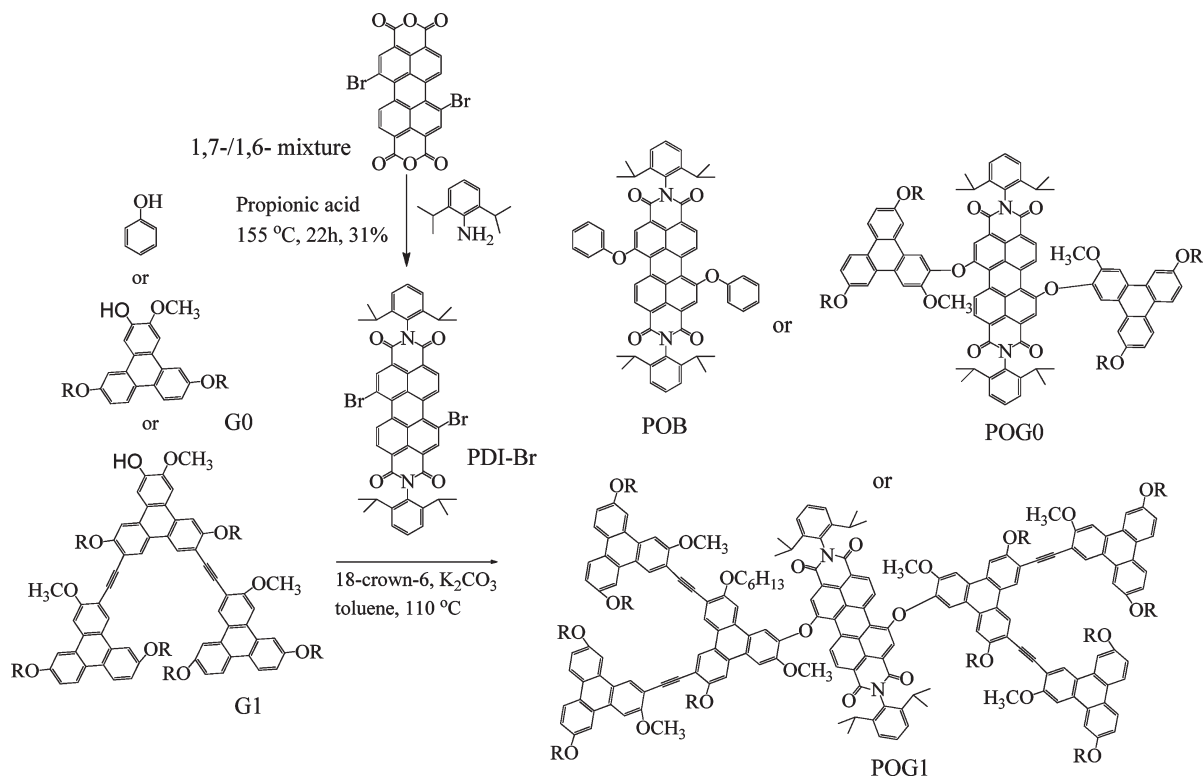
their strong electron accepting<sup>11</sup> and fast electron transporting properties<sup>12</sup> but also due to their remarkable chemical and thermal stability.<sup>13</sup> As one of the best n-type organic semiconductors, PDI derivatives have found extensive applications in organic field effect transistors,<sup>14</sup> light emitting diodes,<sup>15</sup> sensors,<sup>16</sup> and solar cells.<sup>17</sup> An attractive feature of PDI is that its optical properties can be easily fine-tuned by proper substitution in either the bay positions and/or the imide positions, leading to chromophores absorbing a broad section of the visible spectrum.<sup>18</sup> In addition to the large absorption cross section in the visible to near-infrared (IR) region, many PDIs also exhibit strong fluorescence with quantum yields near unity.<sup>19</sup> Thus, PDIs have been extensively used as the energy and electron acceptor in a variety of light harvesting architectures such as rigid linear arrays,<sup>20</sup> molecular squares,<sup>21</sup> as well as supramolecular assemblies.<sup>22</sup>

The combination of light harvesting dendrimers as energy/electron donor and a PDI derivative as the acceptor constitutes an attractive D-A system. Indeed, some pioneering research

**Received:** September 7, 2010

**Revised:** January 13, 2011

**Published:** February 10, 2011

Scheme 1. Synthesis of POG $n$  Dendrimers (R = Hexyl)

along this line has been reported.<sup>23,24</sup> In particular, Müllen et al. have reported PDI derivatives bearing polyphenylene dendrimers of various sizes at either the imide positions or the bay positions.<sup>24</sup> The shape-persistent, three-dimensional polyphenylene dendrimers not only serve as the light harvester, but also form an effective shield on the central PDI core, preventing its self-quenching. Such D-A systems are thus ideal for the study of energy transfer and photoinduced electron transfer at the single molecular level<sup>25</sup> and for generating highly fluorescent dyes.<sup>26</sup>

For applications in molecular electronics, the ability of the PDI core to aggregate/stack is essential as that entails high electron mobility and thus good electron conductivity along the stacked PDI columns.<sup>27</sup> If the donor component can also form stacked separated columns which transport holes, the resulting D-A system may be ideal for photovoltaic applications. Thus, PDI derivatives bearing discotic mesogens as the donor components could be novel new D-A systems. In this paper, we report such a system where a PDI core is covalently linked with triphenylene units or triphenylene-based dendrons. Triphenylene derivatives are planar fused  $\pi$ -systems and one of the most common discotic mesogens.<sup>28</sup> Conjugated dendrons based on triphenyleneacetylenes (TPA) have been shown to exhibit efficient light harvesting property.<sup>29</sup> They also have a high tendency to form  $\pi$ -stacked aggregates. Here we describe the synthesis and characterization of two PDI–triphenylene D-A systems, POG0 and POG1. We report on their photophysical properties in different solvents and as solid films. We demonstrate that electron transfer is dominant in POG1, whether in a polar or a nonpolar solvent, which quenches more than 98% of both the donor and the acceptor fluorescence. For POG0, the electron transfer is efficient only in a

polar solvent. Aggregation is evident in hexane and in the solid film. For POG0, both the PDI core and the triphenylene ring appear to aggregate homotopically, likely forming separated PDI-stack columns and triphenylene columns. For POG1, the aggregation of the triphenylene dendron is evident while the PDI core aggregation is limited, presumably due to the steric hindrance caused by bulky triphenylene moieties which block the access to PDI core.

## RESULTS AND DISCUSSION

**Synthesis.** Scheme 1 shows the structures of POG0 and POG1 and their synthetic approaches. The synthesis of triphenylene based G0 and G1 has been previously reported.<sup>29</sup> Direct bromination of perylene dianhydride yielded an insoluble mixture of 1,7- and 1,6-dibrominated perylene dianhydrides.<sup>30</sup> Without separation, the mixture was subjected to subsequent imidization with 2,6-diisopropylaniline. The resulting PDI derivatives are soluble in common organic solvents. <sup>1</sup>H NMR spectrum analysis gave 1,7-/1,6- isomeric ratio of 4:1. The pure isomer, *N,N'*-bis-(2,6-diisopropyl)phenyl-1,7-dibromo-3,4,9,10-perylene diimide (PDI-Br), was isolated by recrystallization in hot toluene. POG0 and POG1 were prepared by the nucleophilic substitution of PDI-Br with G0 and G1, respectively. While POG0 was synthesized in good yields, the reaction of G1 with PDI-Br was found to be quite complicated. With an excess amount of G1 and the base, and extended reaction time, the reaction still yielded a mixture of both mono- and disubstituted products, which complicates the purification and isolation of the desired product. Repeated column chromatography was needed to isolate the pure disubstituted product. For comparison, a model compound POB was also synthesized by reacting PDI-Br with phenol.

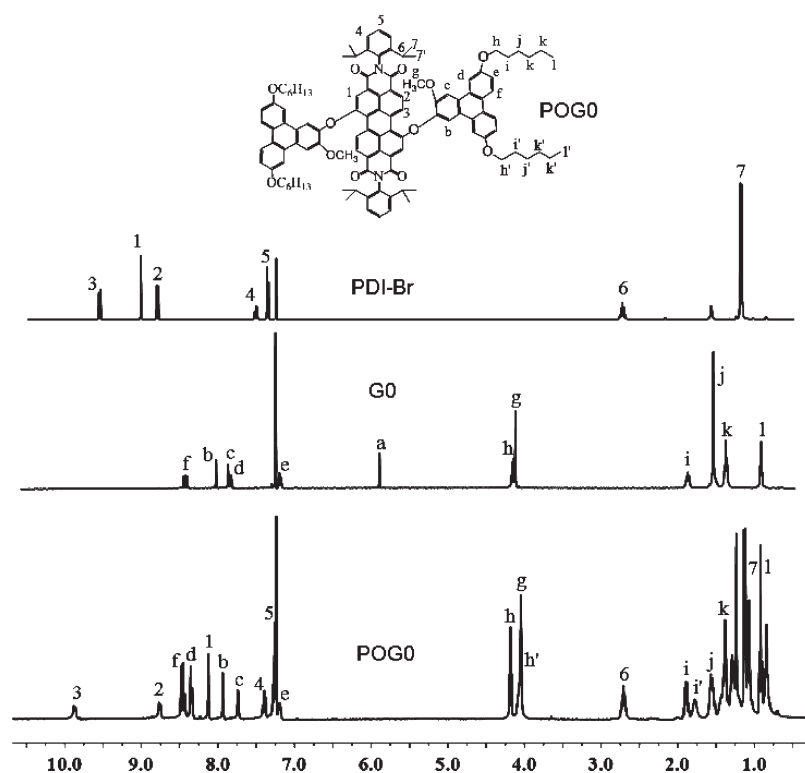


Figure 1.  $^1\text{H}$  NMR spectra of PDI-Br, G0, and POG0 in  $\text{CDCl}_3$ .

**Structural Characterizations.** All dendrimers including the model compound are soluble in common organic solvents such as chloroform, dichloromethane, THF, and DMF. Their structures and purity are confirmed by thin layer chromatography,  $^1\text{H}$  and  $^{13}\text{C}$  NMR, matrix-assisted laser desorption/ionization time-of-flight (MALDI-TOF) mass spectrometry, and elemental analysis.  $^1\text{H}$  NMR spectrum of POG0 gives adequately dispersed signals. As shown in Figure 1, the  $^1\text{H}$  NMR spectrum of POG0 includes signals that can be clearly distinguished from either the triphenylene ring (for example, signals e–g) or the PDI component (for example, signals 2 and 4–6) with negligible changes in chemical shifts. There are, however, notable changes in some proton signals. When PBI-Br is converted to POG0, protons 1, which are closest to the connection site are affected the most with an upfield shift of 0.89 ppm. The significant upfield shift reflects the electron donating nature of the aryl oxygen substituent versus the electron withdrawing effect of the bromo atom. Protons 3, on the other hand, show a moderate downfield shift of 0.33 ppm. Such a downfield shift may be attributed to the intramolecular hydrogen bonding between proton 3 and the ether oxygen. Changes in chemical shifts for protons 4 and 5, which are not part of the central perylene ring, are minimal. It is interesting to note that alkyl protons h and i, each giving one signal in the  $^1\text{H}$  NMR spectra of G0, split into two well-separated signals with a 1:1 integration ratio. One set (labeled as h, i in Figure 1) is sharp with clearly resolved multiplicity, while the other (h' i') is broad (see Supporting Information for the expanded spectrum). The broad signals are upfield shifted compared to the sharp signals. The signal corresponding to proton 7, which gives one doublet in the  $^1\text{H}$  NMR spectrum of PDI-Br, also splits into two signals in POG0, both of which are doublet. Molecular modeling shows that the triphenylene ring may back-bent toward the PDI core but does not reach directly over the PDI plane. One hexyloxy chain can stretch above and across

the PDI  $\pi$ -system, while the other extends away from it. The outward extending hexyl chain likely gives sharp proton NMR signals, while the inward pointing hexyl chain experiences varied shielding effect of the PDI  $\pi$ -system, leading to broad and upfield shifted signals (see Figure S6A for snapshots of molecular dynamics simulation).

While POG0 gives sharp and resolved  $^1\text{H}$  NMR signals, POG1 shows widespread overlapped and clustered signals (see Supporting Information for the spectrum), indicating strong aggregation.<sup>31</sup> Our MD simulation results suggest that such a strong aggregation might come from the stacking interactions between two neighboring triphenylene groups of G1. The G1 substituents on both sides of the PDI core adopt a conformation that is almost perpendicular to the PDI core of POG1. The net result is that the PDI core of POG1 appears to be “protected” by the G1 dendrons (Figure S6B in SI). Because the  $^1\text{H}$  NMR spectrum of POG1 provides little information about the purity of the product, a MALDI-TOF MS analysis was performed. As shown in Figure 2, only one signal at 3686.62 that corresponds to  $M + \text{Ag}^+$  (3686.51) is observed, confirming the structure of POG1. Elemental analysis results further confirmed the structures and purity of POG0 and POG1 (see Experimental Section).

**Photophysical Properties.** The optical properties of all compounds were studied in dilute chloroform solutions, hexane solutions, and as solid films. The results are summarized in Table 1 and discussed in the following sections.

G0, G1, and POB serve as model compounds for investigating optical properties of POG0 and POG1. Thus, their optical properties are presented first before the optical properties of POG0 and POG1 are discussed.

Figure 3 shows the absorption (Figure 3a), excitation (Figure 3b), and emission (Figure 3c) spectra of G0 in chloroform (black), hexane (blue), and as pristine solid films (red). The strongest absorption band of G0 in chloroform is observed at 276 nm, which is

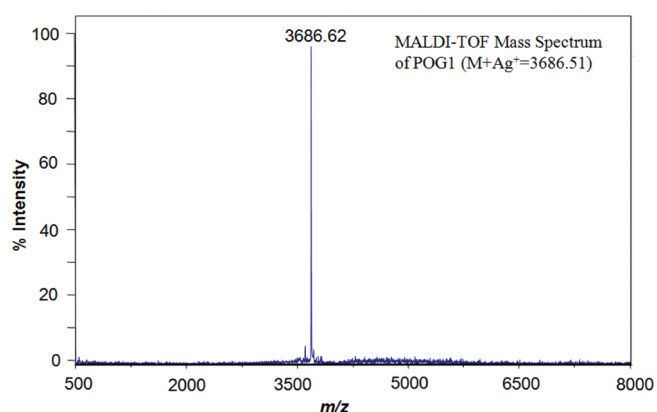


Figure 2. MALDI-TOF mass spectrum of POG1.

Table 1. Optical Properties of G0, G1, POB, POG0, and POG1 in Dilute Chloroform, Hexane, and as Solid Films

		$\lambda_{\text{ab}}$ (nm) <sup>a</sup>	$\lambda_{\text{ex}}$ (nm) <sup>b</sup>	$\lambda_{\text{em}}$ (nm) <sup>c</sup>	$\phi^d$
G0	in CHCl <sub>3</sub>	276	276	365	0.021
	in hexane	272	272	362	0.034
	film	280	272	366	
G1	in CHCl <sub>3</sub>	398	398	407	0.55
	in hexane	393	394	400	0.32
	film	408	408	470	
POB	in CHCl <sub>3</sub>	540	540	571	1.0
	in hexane	526	526	553	1.0
	film	550	555	623	
POG0	in CHCl <sub>3</sub>	272, 556	276	366	<0.001
			518	572	0.025
	in hexane	272, 544	274	361, 560	0.01
			516	560	0.37
	film	286, 582	286	441	
			580	631	
POG1	in CHCl <sub>3</sub>	400, 558	360	409	0.013
			518	575	0.001
	in hexane	408, 565	360	402	0.003
			518	561	<0.003
	film	408, 572	572		

<sup>a</sup> Maximum absorption wavelength. <sup>b</sup> Excitation wavelength used to measure fluorescence emissions and fluorescence quantum yields. <sup>c</sup> Maximum emission wavelength. <sup>d</sup> Fluorescence quantum yield.

attributed to the symmetry-allowed S0–S4 electronic transition.<sup>32</sup> The symmetry-forbidden S0–S1 transition gives bands at 344 and 362 nm with much lower intensity. In hexane, G0 shows similar absorption bands, except for a slight (~2 nm) blue shift. G0 film, on the other hand, gives slightly red-shifted bands and no new bands are observed, which indicates the lacking of strong ground state  $\pi$ – $\pi$  stacking among triphenylene rings. Nonetheless, the aggregation of triphenylene rings, perhaps through hydrogen bonding of the hydroxyl group, is evident as the intensity of the long wavelength absorption bands is increased.<sup>32b</sup>

G0 is only weakly fluorescent. Its fluorescence quantum yields in chloroform and hexane are 0.021 and 0.034, respectively. G0 film, however, is moderately fluorescent. Its fluorescence spectrum shows, interestingly, multiple well-resolved peaks at 366, 384, 404, 430, 458, and 485 nm (Figure 3c). The four lower

wavelength bands can be identified in the solution emission spectra, which thus can be attributed to the fluorescence emission of the nonaggregated G0 molecule. The two long wavelength emission bands (458 and 485 nm) are clearly new emission bands, resulting from a different exciton, which is tentatively assigned to excimers. Taking 384 nm as the emission wavelength, the excitation spectra of G0 in chloroform, hexane, and as a film are shown in Figure 3b. The excitation spectrum of G0 film at the emission wavelength of 458 nm is also shown in Figure 3b. One can notice the matching of the bands observed in the excitation spectra to those seen in the corresponding absorption spectra. For G0 film, the excitation spectra, whether measured at the monomeric emission wavelength (384 nm) or the excimer emission wavelength (458 nm), are again matched to the absorption bands. These results again indicate that there is no strong ground state  $\pi$ – $\pi$  aggregate formation. It is noted that the intensities of the long wavelength bands at 364, 346, and 325 nm are much stronger in the excitation spectra of G0 film than those in the absorption spectra. A sharp excitation band is observed at 363 nm with a half intensity bandwidth less than 10 nm. It is likely that the monomeric emission comes from S1 exciton and the excimer formation also originates from the monomer's S1 excited state. Direct S0–S1 excitation thus leads to stronger fluorescence emissions.

To further help interpret the G0 film emission, the emission spectra of G0 in chloroform at different concentrations were measured. As shown in Figure 4, at concentrations lower than  $10^{-5}$  M, G0 gives only monomer emissions with two clearly resolved bands at 366 and 383 nm and two shoulder bands around 405 and 430 nm. As the concentration increases, the intensity of these emission bands decreases while a new broad band in the longer wavelength range appears. An isoemissive point appears to exist within the studied concentration range, indicating the existence of two emitting species, which interconvert.<sup>33</sup> When the ratio of emission intensity at 464 nm corresponding to the new emission species over that at 384 nm, which is attributed to the monomeric emission species ( $M^*$ ), is drawn over G0 concentration, a linear relationship is obtained (Figure 4, inset). These results are consistent with the view that the red-shifted emissions are dynamic excimer emissions where the excimers are formed by the association of an excited monomer ( $M^*$ ) and a ground state monomer ( $M$ ),  $M^* + M \rightarrow M_2^*$ , instead of static excimer emissions ( $2M \rightarrow M_2^*$ ).<sup>34</sup> The excimer emission bands are broader and not well resolved in solutions. However, one can still identify two humps. When deconvoluted into Gaussian curves, two maxima at 464 and 490 nm are obtained, consistent with those seen in film emissions. One may thus conclude that G0 film shows both monomeric and excimer emissions.

G1 has three triphenylene units joined together by acetylene bonds. Figure 5 shows the absorption (a), emission (c), and excitation (b) spectra of G1 in chloroform (black), hexane (blue), and as a solid film (red). Unlike G0, G1 possesses much stronger absorption in the 300–400 nm wavelength range and is strongly fluorescent in chloroform solution with a quantum yield of 0.55. When the solvent is changed from chloroform to hexane, one observes a slight but clear blue shift in the longest wavelength absorption peak (398 to 393 nm), maximum emission wavelength (407 to 400 nm), and the longest wavelength excitation band (398 to 394 nm). The fluorescence quantum yield is decreased to 0.32. A careful inspection of the absorption and emission spectra of G1 in hexane shows that, while the

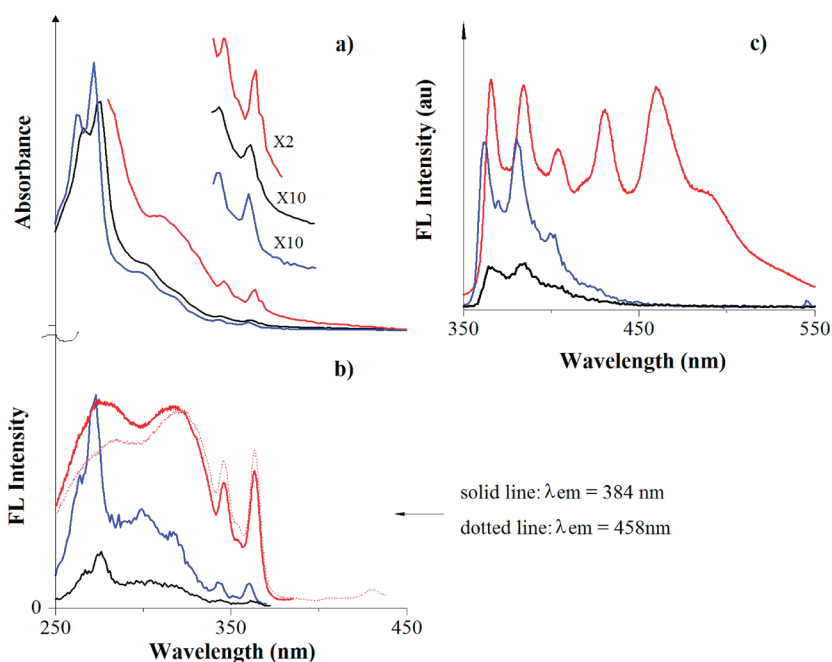


**Figure 3.** UV/vis absorption (a), fluorescence excitation (b), and fluorescence emission (c) spectra of G0 in chloroform (black), hexane (blue), and as solid films (red). The solution concentration is  $1 \times 10^{-6}$  M.

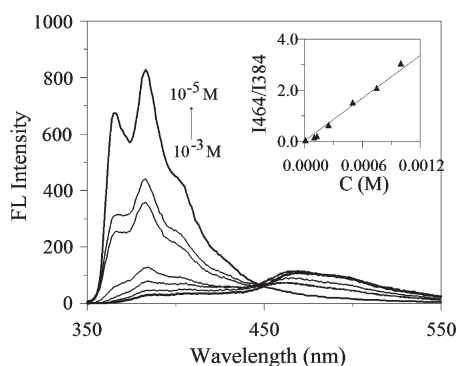


**Figure 4.** Fluorescence emission spectra of G0 in chloroform at different concentrations. The inset shows the emission intensity ratio at 464 nm over 384 nm vs G0 concentrations.

absorption and emission maxima are blue-shifted, there are clearly tails extending to longer wavelengths in both spectra, indicating the existence of some aggregation. Such aggregation perhaps accounts for the decreased fluorescence quantum yield of G1 in hexane. Compared to its chloroform solution, G1 film shows red-shifted absorption, emission, and excitation bands. The extent of redshift is much larger than that observed for G0. Two factors may contribute to the observed red-shift of G1 film: one is the planarization of the G1 dendron and the other is the interdendron aggregation.

Like other PDI derivatives, POB in dilute chloroform or hexane solutions shows intense absorption in the visible range and is highly fluorescent with unity fluorescence quantum yield. As shown in Figure 6, compared to what is observed in G0 or G1, clear and significantly larger blue-shifts in absorption (14 nm), emission (17 nm), and excitation (14 nm) wavelengths are observed when the solvent is switched from chloroform to hexane, indicating a stronger charge transfer character of the

PDI core exciton. All spectra of POB films are again red-shifted. It is noted from the excitation spectra (Figure 6b) that exciting at wavelengths below 400 nm yields negligible fluorescence.

After presenting the optical properties of the individual donor (G0, G1) and acceptor (POB) components, we now move on to discuss the photophysical properties of their D-A systems. The absorption spectrum of POG0 (Figure 7) in chloroform shows multiple bands beyond 450 nm, which are attributed to the PDI core. Compared to POB, the PDI core absorption of POG0 is red-shifted. The  $\lambda_{max}$  in the visible region for POB and POG0 are 540 and 566 nm, respectively. Such a red-shift reflects an increasing electron donating nature from phenyl ether to the triphenylene ether substituents. In the UV region, POB and POG0 all show one relatively sharp and strong band at around 270 nm. When expanded, multiple weak peaks at 349 and 365 nm, corresponding to triphenylene's symmetry forbidden S0–S1 transitions, are discernible. When the solvent is changed from chloroform to hexane, the maximum absorption wavelength in the visible range is clearly blue-shifted, while negligible changes are observed in the UV region. A clear tail extending beyond 600 nm is noted, which is not seen in the absorption spectrum of POB in hexane. The absorption spectrum of the POG0 film shows much broader absorption in both the UV region and the visible region. The maximum absorption wavelength in the visible range of POG0 film is 26 nm red-shifted compared to that of POG0 in chloroform. Such a red-shift is significantly larger than what is observed for POB (10 nm). POG0 film also shows a much broader absorption tail extending to longer wavelengths than POB films. These results indicate that the PDI core of POG0 aggregates differently from that in POB. The much broader absorption and much larger red-shift observed in POG0 films indicate that the PDI core in POG0 either aggregates much more strongly with the PDI core of another POG0 molecule or aggregates heterotopically with the G0 unit. In the 300–450 nm region, one can identify a small but clear peak at around 365 nm and one broad band at around 400 nm, both of which are also observed in POG0s solution spectra.

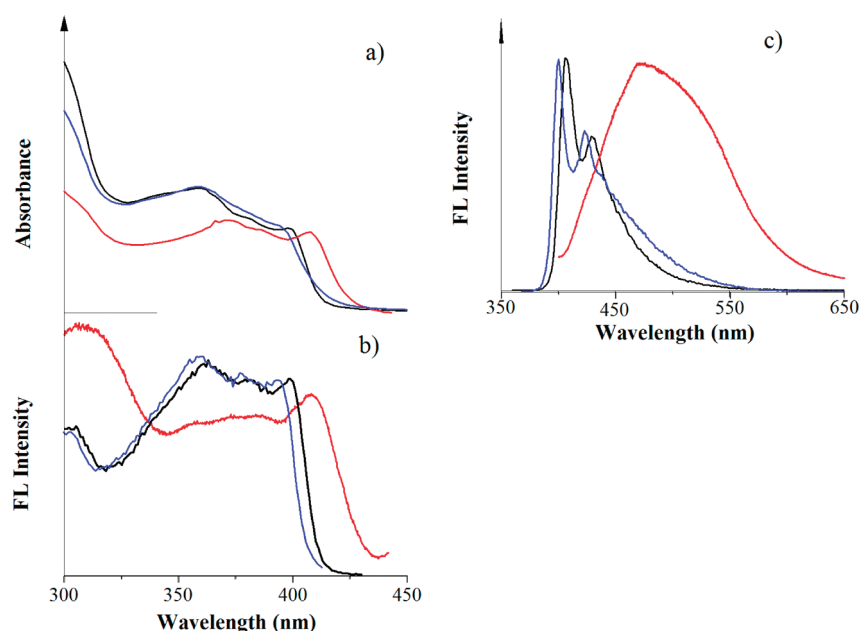


**Figure 5.** UV/vis absorption (a), fluorescence excitation (b), and fluorescence emission (c) spectra of G1 in chloroform (black), hexane (blue), and as solid films (red). The solution concentration is less than  $1 \times 10^{-6}$  M.

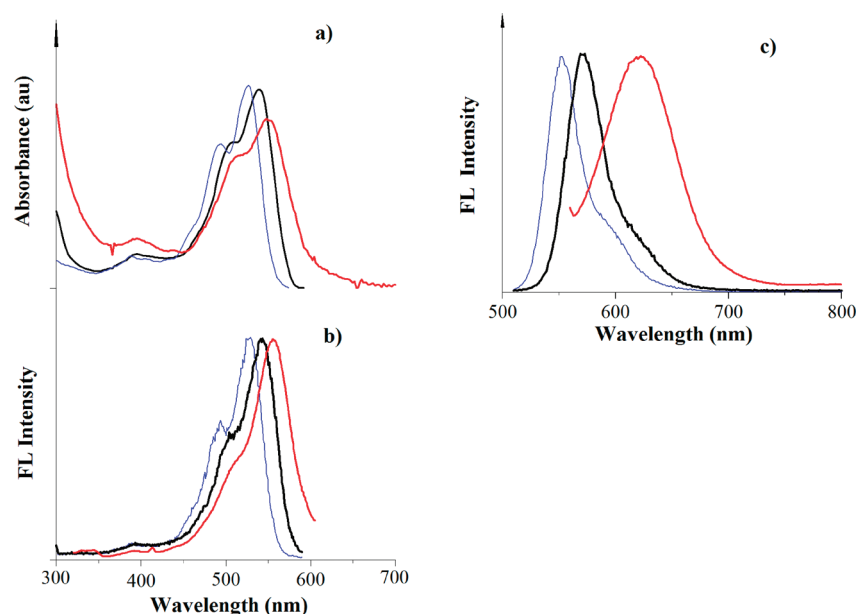


**Figure 6.** UV/vis absorption (a), fluorescence excitation (b), and fluorescence emission (c) spectra of POB in chloroform (black), hexane (blue), and as solid films (red). The solution concentration is less than  $1 \times 10^{-6}$  M.

The lack of new absorption bands in POG0 films appears to indicate that the PDI core and the G0 unit aggregate homotopically (G0 stacking with G0, while PDI stacks with PDI). The absorption tail observed in the hexane solution of POG0 indicates that such aggregation exists, although to a much lesser extent, in the hexane solution.

As mentioned earlier, G0 is only weakly fluorescent, while POB is highly fluorescent. When G0 and the PDI core are covalently linked, both the G0 emission and the PDI core emission are nearly completely quenched when a dilute chloroform solution of POG0 is studied. The fluorescence quantum

yields of POG0 in chloroform with G0 excitation (274 nm) and PDI core excitation (516 nm) are 0.001 and 0.025, respectively, indicating over 95% of the G0 emission and PDI emission are quenched. The fluorescence quenching of the PDI emission is, however, significantly lower in hexane. As shown in Figure 8, when the PDI core of POG0 is excited at 516 nm, the PDI emission intensity is 2 orders of magnitude higher in hexane than that in chloroform. The fluorescence quantum yield of POG0 in hexane at 516 nm is 0.37, compared to 0.025 in chloroform. When excited at 274 nm, POG0 in chloroform shows weak emissions from both the G0 component (emissions in the 350–450 nm range) and the PDI

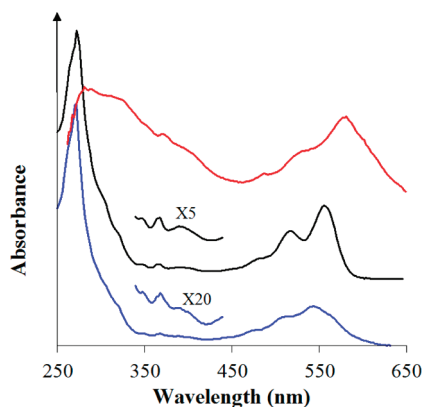


**Figure 7.** UV/vis absorption spectra of POG0 in chloroform (black), hexane (blue), and as solid films (red).

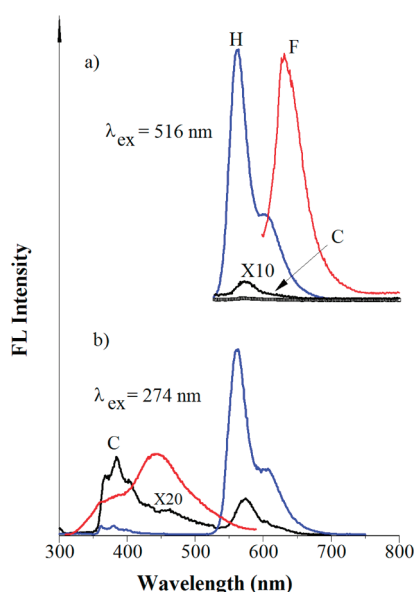


**Figure 8.** Fluorescence emission spectra of POG0 excited at 516 nm (a) and 274 nm (b) in chloroform (black), hexane (blue), and as solid films (red).

component (emissions beyond 500 nm) with G0 emission dominant. In hexane, while the G0 emission is only slightly increased, the PDI emission is again enhanced by orders of magnitude and now strongly dominates the POG0 emission (Figure 8b).

When a POG0 film is excited at 274 nm, a broad emission from 320 to 550 nm is observed (Figure 8b). The broad peak around 450 nm matches well with G0 excimer emission while the shoulder band around 350 nm can be attributed to nonaggregated G0 emission. The fact that similar monomer and excimer emissions are observed for POG0 film and G0 film indicates that the G0 component in POG0 aggregates through G0–G0 stacking. When PDI core is excited, POG0 film gives significantly red-shifted emissions with a  $\lambda_{\text{max}}$  at 631 nm. The extent of red-shift ( $\sim 70$  nm) is comparable to that of POB. These results again indicate that in a POG0 film, the aggregation likely occurs homotopically with triphenylene rings stacked with each other, while PDI cores are aggregated with PDI core.

The absorption spectra of POG1 in chloroform show well structured bands associated with the PDI core and the G1

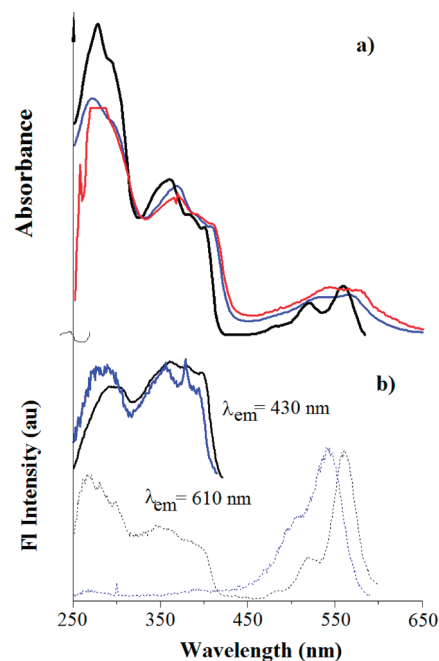


**Figure 9.** UV/vis absorption (a) and fluorescence excitation (b) spectra of POG1 in chloroform (black), hexane (blue), and as solid films (red). The solution concentration is less than  $1 \times 10^{-6}$  M.

dendrons (Figure 9a). The PDI core absorption has a  $\lambda_{\text{max}}$  of 558, nearly identical to that of POG0, indicating that extended conjugation in G1 has negligible effect on the electronic states of PDI core. The extended  $\pi$ -system in G1 leads to the broad absorption in the 300–450 nm range, while the strong bands in the 250–300 nm range can be attributed to the  $\pi$ – $\pi^*$  transition of the individual triphenylene rings. When the absorption spectra of POG1 in different solvents are compared, one sees quite different solvent effect for POG1 from those of G1, POB, and POG0. Instead of blue shifts observed for all those compounds, POG1 exhibits red shift in both the G1 absorption region and the PDI core region when the solvent is changed from chloroform to hexane. The absorption spectrum of POG1 in hexane resembles closely that of its film. Clearly, POG1 is strongly aggregated in hexane, even in highly dilute solutions. It is noted that POG1 in hexane, POG1 film, and G1 film all give nearly identical absorption bands in the 300–450 nm range, indicating that POG1 in hexane or in solid film aggregates mostly through G1–G1 stacking. From chloroform to film, the PDI core absorption of POG1 is red-shifted by 14 nm, while the red shift for POG0 is 38 nm. The much smaller red shift observed for POG1 indicates that PDI–PDI aggregation in POG1 is very limited. Apparently, the bulky G1 substituents at the bay area effectively block the approaching of two PDI cores, consistent with the previously stated molecular dynamics simulation studies.

As mentioned earlier, both G1 and POB are highly fluorescent in dilute chloroform solutions. The fluorescence quantum yields for G1 and POB are 0.545 and 1.0, respectively. When G1 is covalently linked to the PDI core, emissions from both the G1 portion and the PDI core are nearly completely quenched. As shown in Figure 10, POG1 emissions, when measured under identical conditions to those of G1 and POB (same absorbance at the excitation wavelength and the same excitation/emission slit width), are barely observable whether the G1 portion is excited

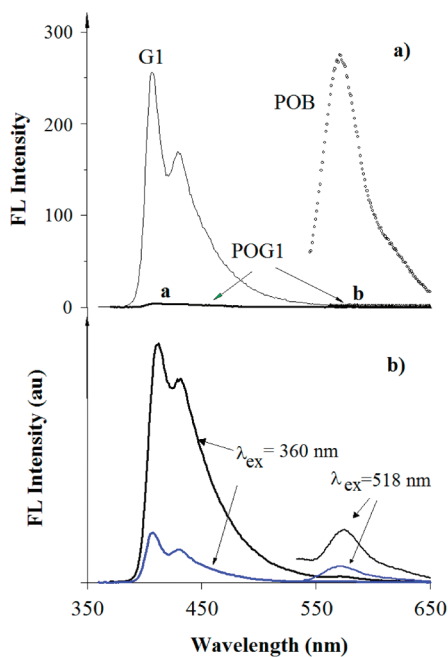


**Figure 10.** Fluorescence emission spectra of G1, POB, and POG1 in chloroform, measured under identical conditions (a). Bottom figure shows the scaled-up emission spectra of POG1 in chloroform (black) and hexane (blue) with donor (360 nm) and acceptor excitations (518 nm).

(at 360 nm) or the PDI core is excited (at 518 nm). The fluorescence quantum yields of POG1 with G1 excitation (360 nm) and PDI excitation (518 nm) are 0.013 and 0.001, respectively, indicating that 98% of the G1 emission and over 99% of PDI emission are quenched. In hexane, the fluorescence emissions of both G1 and PDI core of POG1 are further quenched. The quantum yields are only 0.003 at 360 nm excitation and less than 0.0001 at 558 nm excitation. No fluorescence is detected for POG1 film. As far as the emission wavelengths are concerned, the donor emission of POG1 matches those of G1 while the acceptor emission of POG1 matches those of POB. It is worth noting that, while the PDI core absorption of POG1 is red-shifted by 18 nm compared to that of POB, the PDI emission of POG1 is only red-shifted by 4 nm. A similar phenomenon is also observed for POG0. In other words, POG0 and POG1 exhibit much smaller Stokes shift (16 nm) than that of POB (30 nm), indicating that the excited PDI core in POG0 and POG1 has much less flexibility to reorganize to a lower energy state prior to photoemission. It has been shown that the more distorted the PDI core, the higher the Stokes shift.<sup>35</sup> However, one would not expect the PDI core in POG0 and POG1 to be less distorted than that of POB, considering the bulkiness of the G0 and G1 substituents. Structures from chloroform-based MD simulations suggest that the PDI cores in POG0 and POG1 were quite stable during the 4000 ps MD simulations (Figure S6) and that the bulky G1 appears to have little effect on the PDI core conformation because the conformation of G1 extends away from the PDI core (Figure S7).

Taking 430 nm as the emission wavelength (donor G1 emission), the excitation spectra of POG1 in chloroform and hexane are measured (Figure 9b). In chloroform, the excitation spectrum of POG1 matches well with its absorption spectrum in the 300–420 nm range. In hexane, however, the excitation spectrum of POG1 does not match its absorption spectrum,

**Table 2.** Fluorescence Lifetimes for G0, G1, POB, POG0, and POG1, Measured at 400, 425, 575, 575, and 575 nm, Respectively<sup>a</sup>

compd	A <sub>1</sub>	τ <sub>1</sub> (ns)	A <sub>2</sub>	τ <sub>2</sub> (ns)	A <sub>3</sub>	τ <sub>3</sub> (ns)	τ <sub>avg</sub> (ns)
G0	0.10	8.38	0.32	0.91	0.58	3.37	3.07
G1	1.0	3.71					3.71
POB	1.0	4.60					4.60
POG0	0.995	0.008	0.0040	0.45	0.0010	5.43	0.015
POG1	0.994	0.011	0.0047	0.56	0.0013	4.16	0.019

<sup>a</sup>τ<sub>avg</sub> is the weighted average life time.

but that of G1. When the PDI core emission (610 nm) is taken as the emission wavelength, the excitation spectrum of POG1 in chloroform shows two excitation regions, one with direct PDI core excitation (450–600 nm range) and the other with G1 excitation (250–430 nm region). G1 excitation apparently can lead to PDI core excitation through Förster energy transfer. In hexane, the excitation spectrum of POG1 shows only the PDI core excitation component. The G1 excitation leads to no PDI emission, which is in sharp contrast to what is observed for POG0. As mentioned earlier, POG1 is strongly aggregated in hexane through G1–G1 stacking. It is likely that G1 excitons are deactivated by subsequent energy transfer and photoinduced electron transfer to the PDI core and by self-quenching of aggregation. As far as emission and excitation wavelengths are concerned, the emissions of POG1 resemble G1 (in the G1 emission portion) and POB (in the PDI emission region), indicating that the residual emissions observed on POG1 are due to nonaggregated individual POG1 molecule.

The fluorescence dynamics of G0, G1, POB, POG0, and POG1 were measured in chloroform using the technique of time-correlated single photon counting (TCSPC). Each of the samples was excited with a ~1–2 ps laser pulse at 300 nm, and the fluorescence decays were monitored at 400 nm for G0, 425 nm for G1, and 575 nm for POB, POG0, and POG1, respectively. The data were analyzed by fitting the transients to a convolution of the instrument response function and a sum of exponential decay functions. The results of the fittings along with the weighted average of the time constants (τ<sub>avg</sub>) are collected in Table 2. The fluorescence decay traces and the fitting curves are also presented in Figure 11. While the fluorescence decay curve of POB was adequately fit to a single exponential decay function with a time constant of 4.60 ns, fitting of the PL dynamics of POG0 and POG1 required a sum of three exponential terms with the overwhelmingly dominant component having a time constant of only around 10 ps. Because our instrument response time is around 40 ps, there is a possible large uncertainty in the “real” fluorescence decay time for POG0 and POG1. Nonetheless, these fits give at least the upper limits to the lifetime. The dramatic shortening of the PDI fluorescence lifetimes after G0 or G1 attachment clearly indicates the existence of a fluorescence quenching mechanism. Because the bandgap of the PDI core is much smaller than that of the G0 or G1, energy transfer from PDI core to the G0 or G1 dendron is not possible. Photoinduced electron transfer is thus presumed to be the major fluorescence quenching pathway for PDI excitons. It should be noted that both POG0 and POG1 were excited at 300 nm, a wavelength where G0 and G1 absorb more strongly than the PDI core does. Should PDI excitons arise significantly from energy transfer from G0/G1 excitons to the PDI core, a growing-in PDI emissions

may be observed. Our fitting procedure involving convolution of the instrument response ( $\sim 40$  ps) with the exponential decay functions fit the very early time part of the data reasonably well. In other words, the fitting did not require a rise time component, which may be attributed to a rise time too fast to be resolved by the TCSPC apparatus. Clearly, it would be desirable to have ultrafast measurements of the fluorescence rise time to fully understand the exciton decay dynamics.

When the donor G0 or G1 is excited, the donor exciton is efficiently quenched for both POG0 and POG1. The fact that enhanced PDI core emission is observed for POG0 in hexane when G0 is excited and the observation that G1 exciton leads to PDI core emission indicate that Förster energy transfer at least

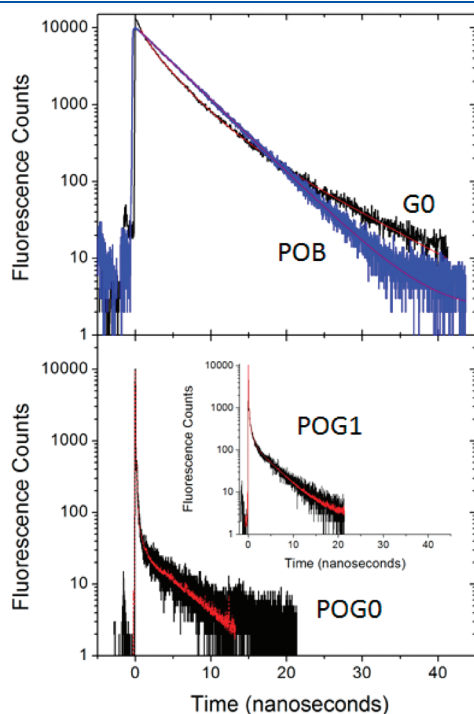


**Figure 11.** Fluorescence decays of G0, POB, POG0 and POG1 in chloroform measured at 400, 575, 575, and 575 nm, respectively, by time-correlated single photon counting ( $\lambda_{\text{exc}} = 300$  nm).

partially accounts for the donor exciton quenching. When POB absorption was used as the PDI core absorption and G0 or G1 emission as the donor emission, the spectral overlap integrals ( $J_F$ ) of POG0 and POG1 were calculated to be  $3.02 \times 10^{-14}$  and  $4.72 \times 10^{-14} \text{ cm}^6 \text{ mol}^{-1}$ , respectively. The energy transfer rate of POG0 and POG1 can thus be estimated using the Förster equation:<sup>36</sup>

$$k_{\text{EN}} = \frac{1}{\tau} \frac{9000(\ln 10) \langle k^2 \rangle \phi}{128\pi^5 N_{\text{av}} n^4 r^6} J_F = \frac{1}{\tau} \left[ \frac{R_0}{r} \right]^6 \quad (1)$$

where  $\tau$  and  $\phi$  are the fluorescence lifetime and fluorescence quantum yield of the donor in the absence of the acceptor,  $J_F$  is the overlap integral between the donor emission and the acceptor absorption,  $\langle k^2 \rangle$  is the orientation factor,  $N_{\text{av}}$  is the Avogadro's number,  $n$  is the refractive index of the medium,  $R_0$  is the Förster radius, and  $r$  is the center-to-center distance of the donor and the acceptor involved in the energy transfer. When the following numbers for POG0 ( $J_F = 3.02 \times 10^{-14} \text{ cm}^6 \text{ mol}^{-1}$ ,  $\tau = 3.07$  ns,  $\phi = 0.021$ ) and POG1 ( $J_F = 4.72 \times 10^{-14} \text{ cm}^6 \text{ mol}^{-1}$ ,  $\tau = 3.71$  ns,  $\phi = 0.55$ ) are used and assuming a random orientation ( $\langle k^2 \rangle \geq 2/3$ ), the Förster radii of POG0 and POG1 were calculated to be 2.1 and 3.9 nm, respectively. Molecular dynamics simulations show that the maximum donor–acceptor (D–A) distances for POG0 and POG1 are 0.89 and 1.53 nm, respectively. In other words, the D–A distances in POG0 and POG1 are much shorter than their respective Förster radii, indicating that the excitonic energy transfer can be efficient. When the maximum D–A distances were used, the low-limit energy transfer rates are calculated to be  $5.6 \times 10^{10} \text{ s}^{-1}$  and  $7.2 \times 10^{10} \text{ s}^{-1}$  for POG0 and POG1, respectively.

To confirm whether or not a charge transfer process, following either the donor excitation or the acceptor excitation, is energetically favorable, the frontier orbitals of POGN were evaluated using cyclic voltammetry measurements. PDI core is fairly electron deficient and thus easy to reduce and difficult to oxidize. G0 and G1, on the other hand, are electron rich and easy to oxidize. During cathodic scan, POB and POG0 both show two reversible reduction waves (Figure 12), which can be attributed to the reduction of the PDI core.<sup>11a</sup> The PDI core of POG0 is slightly more difficult to reduce than that of POB, reflecting the stronger electron-donating property of the triphenylene ether substituent. Based on the half wave potentials ( $-1.17$  V for POB

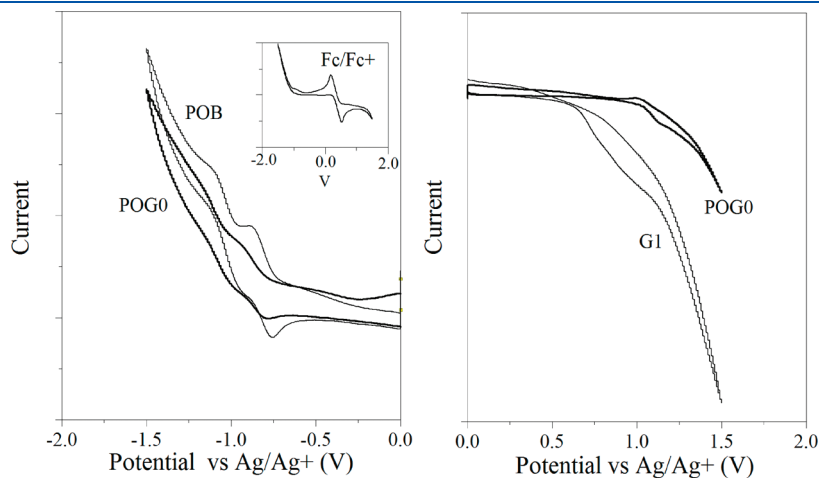


**Figure 12.** Cyclic voltammograms of POB, POG0 on cathodic scan (left), and POG0, G1 on anodic scan (right). Under identical conditions, the ferrocene/ferrocenium couple has a half wave potential of 0.36 V (inset).

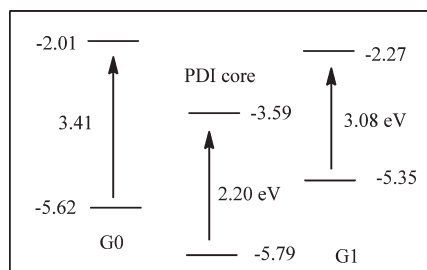


**Figure 13.** Frontier orbitals of the donor (G0 and G1) and the acceptor (PDI core) and their bandgaps.

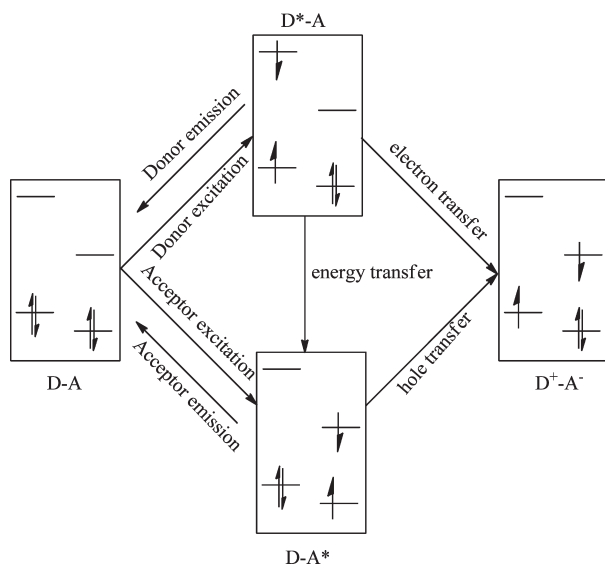


**Figure 14.** Schematic presentation of photophysical processes involved in the D-A system.

and  $-1.22$  V for POG0 vs  $\text{Cp}_2\text{Fe}$ ), the LUMO of the PDI core for POB and POG0 can be calculated to be  $-3.63$  and  $-3.58$  eV, respectively. On the anodic scan, POG0 shows one semireversible oxidation wave, which is attributed to the oxidation of the triphenylene ring. From the half wave potential ( $0.82$  V vs  $\text{Cp}_2\text{Fe}$ ), the HOMO of the donor G0 in POG0 is estimated to be  $-5.62$  eV. Due to insufficient sample, we are not able to obtain the cyclic voltammogram of POG1. It is reasonable to assume though that the oxidation of the G1 component in POG1 is not much different from the oxidation of the separate G1 dendron. Thus, from the oxidation potential of G1 ( $0.55$  V vs  $\text{Cp}_2\text{Fe}$ ), one can estimate the HOMO of POG1 to be  $-5.35$  eV. Similarly, the LUMO of the PDI core in POG1 can be assumed to be the same as that of POG0. Combining the electronic bandgaps of G0, G1, POG0, and POG1, which can be obtained from their absorption and fluorescence emission spectra, the frontier orbitals of the donor component and the acceptor PDI core are calculated and are shown in Figure 13.

When donor G0 or G1 is excited, one sees a facile electron transfer from excited donor to the LUMO of the acceptor, leading to a nonemissive charge-separated state (Figure 14). One competing pathway is the deactivation of the donor exciton through Förster energy transfer, leading to acceptor excitation, which can be subsequently quenched by charge transfer. When the acceptor PDI core is excited, there is a facile hole transfer

**Table 3.** Change in Free Energy for Charge Separation  $\Delta G_{\text{cs}}/\text{eV}$  from Donor Excitation and Acceptor Excitation<sup>a</sup>

solvent	$\Delta G_{\text{POG0}}(\text{D}^*)$	$\Delta G_{\text{POG0}}(\text{A}^*)$	$\Delta G_{\text{POG1}}(\text{D}^*)$	$\Delta G_{\text{POG1}}(\text{A}^*)$
chloroform	$-1.72$	$-0.51$	$-1.52$	$-0.64$
hexane	$-1.18$	$0.03$	$-1.01$	$-0.13$

<sup>a</sup>  $e = 1$ ,  $\epsilon_0 = 0.055 \text{ eV}^{-1} \text{ nm}^{-1}$ ,  $\epsilon_s = 4.81$  (chloroform),  $1.89$  (hexane),  $\epsilon_{\text{ref}} = 4.81$  (chloroform),  $(E_{\text{ox}} - E_{\text{rd}})^{\dagger} = 2.03$  for POG0 and  $1.76$  for POG1,  $E_{00}(\text{G0}) = 3.41$  eV,  $E_{00}(\text{G1}) = 3.08$  eV,  $E_{00}(\text{PDI}) = 2.20$  eV.

pathway that moves the hole from the HOMO of PDI to the HOMO of G1, again leading to the same nonemissive charge separated state. Thus, no matter if the donor or the acceptor is excited, photoinduced electron (or hole) transfer follows that quenches both the donor and the acceptor fluorescence and leads to a nonemissive photoinduced charge separated state.

As shown earlier, fluorescence quenching for POG1 is highly efficient in both chloroform and hexane. POG0, on the other hand, shows efficient fluorescence quenching in chloroform but poor quenching in hexane when the PDI core is excited. Apparently, a photoinduced electron transfer of POG0 with PDI core excitation is highly dependent on the polarity of the solvent, a phenomenon observed on other D-A systems as well.<sup>25,37</sup> Such a strong solvent dependence may be explained by the free energy change ( $\Delta G$ ) associated with the photoinduced charge transfer process, which can be expressed by the Rehm–Weller equation.<sup>38</sup>

$$\Delta G = e(E_{\text{ox}} - E_{\text{rd}}) - E_{00} - \frac{e^2}{4\pi\epsilon_0\epsilon_s R_{\text{cc}}} - \frac{e^2}{8\pi\epsilon_0} \left( \frac{1}{r^+} + \frac{1}{r^-} \right) \left( \frac{1}{\epsilon_{\text{ref}}} - \frac{1}{\epsilon_s} \right)$$

where  $E_{\text{ox}}$  and  $E_{\text{rd}}$  are the oxidation and reduction potential of the donor and the acceptor, respectively,  $E_{00}$  is the excited state energy from which electron transfer occurs,  $\epsilon_s$  is the polarity of the solvent used for spectroscopy studies, while  $\epsilon_{\text{ref}}$  is the polarity of the solvent used to determine the redox potentials,  $R_{\text{cc}}$  is the center-to-center donor–acceptor distance,  $r^+$  and  $r^-$  are the ionic radii of the donor and acceptor dyes, respectively,  $e$  is the electron charge and  $\epsilon_0$  is the vacuum permittivity. When  $r^+(\text{G0}) = 5.14$  Å,  $r^+(\text{G1}) = 11.60$  Å, and  $r^- = 3.75$  Å are used, all of which are estimated from molecular simulations, and assuming  $R_{\text{cc}} = r^+ + r^-$ ,<sup>39</sup> the change in free energy for charge separation was calculated according to the Rehm–Weller equation and are shown in Table 3. Electron transfer is energetically possible for POG1 in both chloroform and hexane, with either donor exciton or acceptor excitation. For POG0, while charge separation is energetically favorable in chloroform, the free energy change is slightly positive in hexane when the acceptor is excited.

To gauge whether kinetics also contributes to the solvent dependence of the charge transfer process of POG0, the rate constant for charge separation is estimated based on the following equation<sup>40</sup>

$$K_{\text{cs}} = \left[ \frac{4\pi^3}{\lambda k_{\text{B}} T h^2} \right]^{1/2} V^2 \exp \left[ \frac{-\Delta G_{\text{cs}}^{\ddagger}}{k_{\text{B}} T} \right]$$

where  $V$  is the coupling between donor and acceptor in the excited state,  $\lambda$  is the reorganization energy, and  $\Delta G_{\text{cs}}^{\ddagger}$  is the barrier for charge separation. The reorganization energy includes internal ( $\lambda_i$ ) and solvent ( $\lambda_s$ ) contributions. For donor–acceptor systems with extended  $\pi$ -conjugation and structural rigidity, the internal nuclear reorganization energy is usually small and  $0.3$  eV is a good estimate.<sup>40</sup> The solvent reorganization energy can be

**Table 4. Solvent Reorganization Energy  $\lambda_s$ /eV and the Barrier for Charge Separation from PDI Excitons in Different Solvents**

	$\lambda_s$		$\Delta G_{cs}^\ddagger$ (with PDI excitation)	
	POG0	POG1	POG0	POG1
hexane	$\sim 0$ (<0.0001)	$\sim 0$ (<0.0001)	0.09	0.024
chloroform	0.46	0.44	0.02	0.003

estimated from<sup>41</sup>

$$\lambda_s = \frac{e^2}{4\pi\epsilon_0} \left[ \frac{1}{2} \left( \frac{1}{r^+} + \frac{1}{r^-} \right) - \frac{1}{R_{cc}} \right] \left( \frac{1}{n^2} - \frac{1}{\epsilon_s} \right)$$

and the results are listed in Table 4, from which the barrier for charge separation is calculated ( $\Delta G_{cs}^\ddagger = (\Delta G_{cs} + \lambda)^2/4\lambda$ ).

The barrier for charge separation for POG1 in both solvents and POG0 in chloroform is low and is only slightly higher for POG0 in hexane. Considering the short donor–acceptor distance for POG0 and POG1, the coupling  $V$  is probably not low and is not likely responsible for the solvent effect. In other words, electron transfer appears to be a kinetically facile process for POG0 and POG1 in both solvents. The dramatic solvent dependence of the electron transfer process of POG0 is thus concluded as a thermodynamic effect, not a kinetic one.

## CONCLUSIONS

A donor–acceptor system containing a perylene diimide core as the acceptor, triphenylene or triphenylene-based conjugated dendrons as the donor has been prepared. Both PDI and triphenylene derivatives are common discotic mesogens which exhibit strong tendency to form  $\pi$ -stacked columnar liquid crystals. In polar solvent chloroform, both POG0 and POG1 exhibit efficient fluorescence quenching when the donor units (G0 and G1) or the PDI acceptor is excited. Photoinduced electron transfer is the dominating mechanism for exciton deactivation when the PDI core is excited, while both excitonic energy transfer and photoinduced electron transfer contribute to the deactivation of the donor excitons. In nonpolar solvent hexane, POG0 and POG1 exhibit different fluorescence quenching behavior. While effective fluorescence quenching is observed for POG1, fluorescence quenching is not effective for POG0 when the acceptor is excited. Theoretical calculations show that the free energy change associated with the charge transfer process for the acceptor exciton is significantly negative for POG1 in both polar and nonpolar solvents, but only appreciably negative for POG0 in chloroform. In other words, charge transfer from acceptor exciton for POG0 in hexane is no longer energetically favored. As pristine films, POG0 is aggregated through G0–G0 and PDI–PDI stacking. When the donor G0 is excited, both monomeric G0 emissions and G0 excimer emissions are observed. For POG1, aggregation occurs mostly through G1–G1 stacking, while the PDI-core is sterically blocked by the perpendicularly oriented bulky G1 substituents. POG1 films exhibit no fluorescence.

## EXPERIMENTAL SECTION

**General Methods.** The syntheses of G0 and G1 were previously reported.<sup>29</sup> All reagents and solvents were obtained from either Aldrich or Fisher and were used as received unless otherwise stated. Anhydrous THF were distilled over sodium/benzophenone.

Triethylamine was distilled from calcium hydride prior to use. All air- and moisture-sensitive reactions were carried out in oven-dried glassware under a nitrogen atmosphere unless stated otherwise.

<sup>1</sup>H and <sup>13</sup>C NMR spectra were recorded on a Varian Unity 400 MHz NMR spectrometer. A Voyager DE Pro (Perceptive Biosystems/ABI) MALDI-TOF mass spectrometer was used for mass measurement, operating in reflector mode. A mixture of silver trifluoroacetate/dithranol (1,8-dihydroxyanthrone; 1:25 w/w) was used as the matrix. UV–vis absorption spectra were recorded in 1 cm path length UV-grade spectrophotometric cells using a Hewlett–Packard 8452A diode array spectrophotometer. The fluorescence emission and excitation spectra were measured using a Shimadzu RF-5301PC spectro-fluorophotometer. All samples were deoxygenated by bubbling N<sub>2</sub> gas through the sample immediately prior to the fluorescence measurements. The slits on the excitation and emission sides of the fluorescence spectrometer have been mentioned in the text. Fluorescence quantum yields were determined by comparing the integrated fluorescence spectra of the compounds with the integrated fluorescence spectrum of the selected standard and correcting for the different refractive indices of the sample and the standard. For G0 and G1 emissions, quinine sulfate in 1 N H<sub>2</sub>SO<sub>4</sub> ( $\Phi_{fl} = 0.55$ ) was used as the standard, while cresyl violet perchlorate in methanol ( $\Phi_{fl} = 0.54$ ) was used as the standard for determining the fluorescence quantum yield of the PDI core emissions. The refractive index of the solvent was used to approximate the sample refractive index, and the refractive index of water was used for the standard (both at 25 °C). The time-dependent fluorescence measurements were performed using the technique of time-correlated single-photon counting (TCSPC). Cyclic voltammetry (CV) studies were carried out in chloroform at room temperature under argon protection using a BAS Epsilon EC electrochemical station employing a 1 mm<sup>2</sup> Pt disk as the working electrode, Ag/AgNO<sub>3</sub> as the reference electrode and a Pt wire as the counter electrode. 0.1 M tetrabutylammonium hexafluorophosphate was the supporting electrolyte, and the scan rate was 50 mV/s. Each measurement was calibrated with ferrocene (Fc) as the internal standard (with the measured  $E_{1/2}^{FC} = 0.355$  V vs Ag/AgNO<sub>3</sub>). In the case of reversible curves, each anodic and corresponding cathodic potential was averaged as  $E_{1/2}^{red/ox} = 1/2(E_{pc} + E_{pa})$  to obtain oxidation and reduction potentials. HOMO and LUMO energy levels were estimated on the basis of the reference energy levels of ferrocene (4.8 eV below the vacuum level) according to  $E_{HOMO}/E_{LUMO} = 4.8 + (E_{1/2} - E_{1/2}^{FC})$  eV below the vacuum level.

**Molecular Dynamics (MD) Simulations.** We used established procedures<sup>42</sup> for MD simulations. Each system (POG0 and POG1) was soaked in a rectangular box of explicit chloroform molecules extended 10 Å away in all directions from any atom of POG0 or POG1, resulting in a POG0 system with 585 chloroform molecules and a box of 42.3 × 40.9 × 47.1 Å, and a POG1 system with 1207 chloroform molecules and a box of 53.3 × 49.6 × 63.9 Å. Each system was minimized for 1000 steps to reduce steric clash, followed by 30 ps of ramping up the temperature from 10 to 300 K. Each system was equilibrated with the NPT ensemble for 100 ps at 300 K, followed by a production run of 4000 ps, collecting 4000 snapshots with the time step of 2 fs. To observe the trajectory changes over time, we minimized snapshots from both systems at the zeroth ps, 2000th ps, and 4000th ps. All energy minimization and MD simulations were carried out using the AMBER 10 package<sup>43</sup> with the AMBER 99SB force field.<sup>44</sup> The minimized structures were listed

in Figure S6. The long-range electrostatic interactions were calculated with the particle mesh Ewald (PME) method<sup>45</sup> and the nonbonded cutoff for the van der Waals interactions was 10 Å.

***N,N'*-Bs-(2,6-diisopropyl)phenyl-1,7-phenoxy-3,4,9,10-perylene Diimide (POB).** Compound PDI-Br (0.02 g, 0.0230 mmol), phenol (0.01 g, 0.1063 mmol), K<sub>2</sub>CO<sub>3</sub> (0.01 g, 0.0724 mmol), 18-crown-6 (0.025 g, 0.0946 mmol), and anhydrous toluene (5 mL) were stirred at 110 °C under nitrogen for 45 min. The resulting mixture was poured into a saturated solution of K<sub>2</sub>CO<sub>3</sub> and then extracted with dichloromethane. The organic extracts were washed with water, dried over anhydrous MgSO<sub>4</sub>, and the solvent was then evaporated. The crude product was purified by flash chromatography eluting with 1:1 dichloromethane/hexane to give the product as a red solid (0.015 g, 73%). <sup>1</sup>H NMR (400 MHz, CDCl<sub>3</sub>): δ 9.65 (d, *J* = 12.0 Hz, 1H), 9.59 (d, *J* = 8.0 Hz, 1H), 8.76 (d, *J* = 8.0 Hz, 1H), 8.70 (d, *J* = 8.0 Hz, 1H), 8.42 (s, 1H), 8.34 (s, 1H), 7.44 (m, 6H), 7.31 (m, 4H), 7.25 (m, 2H), 7.18 (m, 4H), 2.70 (m, 4H), 1.13 (m, 24H). <sup>13</sup>C NMR (400 MHz, CDCl<sub>3</sub>): δ 163.6, 163.4, 162.8, 162.7, 155.9, 155.2, 155.0, 154.9, 145.6, 133.6, 131.8, 130.9, 130.6, 130.4, 129.7, 129.6, 129.0, 128.0, 126.0, 125.1, 124.9, 124.8, 124.7, 124.1, 124.0, 123.9, 122.4, 119.2, 119.0, 29.7, 29.2, 24.0. Anal. Calcd. for C<sub>60</sub>H<sub>50</sub>N<sub>2</sub>O<sub>6</sub>: C, 80.51%; H, 5.63%; N, 3.13%; O, 10.73%. Found: C, 80.07%; H, 5.78%.

**POG0.** PDI-Br (0.0533 g, 0.0614 mmol), G0-OH (0.1064 g, 0.2245 mmol), K<sub>2</sub>CO<sub>3</sub> (0.0264 g, 0.1910 mmol), 18-crown-6 (0.06 g, 0.2270 mmol), and anhydrous toluene (10 mL) were stirred at 110 °C under nitrogen for 18 h. The resulting mixture was poured into saturated solution of K<sub>2</sub>CO<sub>3</sub> and then extracted with dichloromethane. The organic extracts were washed with water, dried over anhydrous MgSO<sub>4</sub>, and the solvent was then evaporated. The crude product was purified by column chromatography eluting with 1:1 dichloromethane/hexane to give the product as a red solid (0.042 g, 42%). <sup>1</sup>H NMR (400 MHz, CDCl<sub>3</sub>): δ 9.86 (d, *J* = 8.0 MHz, 2H), 8.75 (d, *J* = 8.0 MHz, 2H), 8.46 (d, *J* = 8 Hz, 4H), 8.43 (d, *J* = 8.0 Hz, 2H), 8.34 (d, *J* = 8.0 MHz, 4H), 8.12 (s, 2H), 7.94 (d, *J* = 4.0 MHz, 2H), 7.74 (s, 2H), 7.40 (t, *J* = 8.0 MHz, 2H), 7.26 (d, *J* = 8 MHz, 4H), 7.19 (d, *J* = 8.0 MHz, 2H), 4.18 (t, *J* = 6.0 MHz, 4H), 4.05 (br, 10H), 2.71 (m, 4H), 1.89 (m, 4H), 1.78 (br, 4H), 1.57 (m, 8H), 1.38 (m, 16H), 1.12 (d, *J* = 4 Hz, 12H), 1.07 (d, *J* = 4.0 MHz, 12H), 0.92 (t, *J* = 6.0 MHz, 12H). <sup>13</sup>C NMR (400 MHz, CDCl<sub>3</sub>): δ 163.6, 163.0, 157.8, 156.2, 150.9, 145.5, 142.7, 134.1, 130.5, 129.9, 129.5, 129.0, 125.6, 124.9, 124.5, 124.4, 124.1, 123.9, 123.8, 123.4, 122.7, 122.1, 121.6, 116.6, 115.7, 115.5, 115.2, 107.6, 106.8, 68.4, 56.2, 31.7, 29.7, 29.4, 24.0, 29.3, 29.1, 25.8, 25.7, 24.0, 22.7, 22.6, 14.1, 14.0. Anal. Calcd. for C<sub>110</sub>H<sub>114</sub>N<sub>2</sub>O<sub>12</sub>: C, 79.78%; H, 6.94%; N, 1.69%; O, 11.59%. Found: C, 79.62%; H, 7.11%.

**Compound POG1.** PDI-Br (0.0062 g, 0.0071 mmol), G1-OH (0.0414 g, 0.0288 mmol), K<sub>2</sub>CO<sub>3</sub> (0.01 g, 0.0724 mmol), 18-crown-6 (0.019 g, 0.0719 mmol), and anhydrous toluene (5 mL) were stirred for 40 h. The crude product was purified by column chromatography eluting with 1:5 ethyl acetate/hexane. The first fraction was collected and it was then subjected to another column chromatography eluting by 100% dichloromethane to give the first fraction as product (red solid) (0.008 g, 32%). <sup>13</sup>C NMR (400 MHz, CDCl<sub>3</sub>): MALDI-TOF mass analysis calcd for C<sub>242</sub>H<sub>258</sub>N<sub>2</sub>O<sub>24</sub>, 3578.64 (M + Ag<sup>+</sup>: 3686.51); found, 3686.62. Anal. Calcd. for C<sub>242</sub>H<sub>258</sub>N<sub>2</sub>O<sub>24</sub>: C, 81.22%; H, 7.27%; N, 0.78%; O, 10.73%. Found: C, 80.94%; H, 7.49%.

## ■ ASSOCIATED CONTENT

Supporting Information. <sup>1</sup>H and <sup>13</sup>C NMR spectra of the compounds, molecular dynamics (MD) simulations of POG0 and POG1, and additional optical spectra (absorption, fluorescence emission, excitation). This material is available free of charge via the Internet at <http://pubs.acs.org>.

## ■ ACKNOWLEDGMENT

This work is supported by the National Science Foundation (DMR 0804158) and the Army Research Office (W911NF-10-1-0476). We thank Dr. Yi Liu for his help with some of the molecular modeling studies.

## ■ REFERENCES

- (1) (a) Hu, X.; Damjanovic, A.; Ritz, T.; Schulten, K. *Proc. Natl. Acad. Sci. U.S.A.* **1998**, *95*, 5935. (b) Deisenhofer, J.; Norris, J. R., Eds. *The Photosynthetic Reaction Center*; Academic Press: San Diego, 1993.
- (2) (a) Balzani, V., Ed. *Electron Transfer in Chemistry*; Wiley-VCH: Weinheim, 2001. (b) Fox, M. A.; Chanon, M., Ed. *Photoinduced Electron Transfer*; Elsevier: Amsterdam, 1988.
- (3) (a) Carter, F. L., Ed. *Molecular Electronic Devices I, II*; Dekker: New York, 1982, 1987. (b) Petty, M. C.; Bryce, M. R.; Bloor, D., Eds. *An Introduction to Molecular Electronics*; Oxford University Press: New York, 1995.
- (4) (a) Newkome, G. R.; Moorefield, C. N.; Vögtle, F. *Dendritic Molecules: Concepts, Syntheses, Perspectives*, VCH, Weinheim, 1996. (b) Fréchet, J. M. J.; Hawker, C. J. In *Synthesis and Properties of Dendrimers and Hyperbranched Polymers, Comprehensive Polymer Science*, 2nd Suppl.; Aggarwal, S. L., Russo, S., Eds.; Pergamon: Oxford, 1996. (c) Fischer, M.; Vögtle, F. *Angew. Chem., Int. Ed.* **1999**, *38*, 884. (d) Smith, D. K.; Diederich, F. *Chem.—Eur. J.* **1998**, *4*, 1353. (e) Tomalia, D. A.; Naylor, A. M.; Goddard, W. A., III *Angew. Chem., Int. Ed.* **1990**, *29*, 138. (f) Zeng, F.; Zimmerman, S. C. *Chem. Rev.* **1997**, *97*, 1681.
- (5) (a) Nantalaksakul, A.; Reddy, D. R.; Bardeen, C. J.; Thayumanavan, S. *Photosynth. Res.* **2006**, *87*, 133. (b) D'Ambruso, G. D.; McGrath, D. V. *Energy Harvest. Mater.* **2005**, 281. (c) Flomenbom, O.; Klaffer, J.; Amir, R. J.; Shabat, D. *Energy Harvest. Mater.* **2005**, 245. (6) (a) Devadoss, C.; Bharathi, P.; Moore, J. S. *J. Am. Chem. Soc.* **1996**, *118*, 9635. (b) Kopidakis, N.; Mitchell, W. J.; van de Lagemaat, J.; Ginley, D. S.; Rumbles, G.; Shaheen, S. E.; Rance, W. L. *Appl. Phys. Lett.* **2006**, *89*, 103524. (c) Meskers, S. C. J.; Bender, M.; Hubner, J.; Romanovskii, Y. V.; Oestreich, M.; Schenning, A. P. H. J.; Meijer, E. W.; Bassler, H. J. *Phys. Chem. A* **2001**, *105*, 10220. (d) Lu, D.; Feyter, S. D.; Cotlet, M.; Stefan, A.; Wiesler, U. M.; Herrman, A.; Grebel-Koehler, D.; Qu, J.; Mullen, K.; Schryver, F. C. D. *Macromolecules* **2003**, *36*, 5918.
- (7) (a) Peng, Z.; Pan, Y.; Xu, B.; Zhang, J. *J. Am. Chem. Soc.* **2000**, *122*, 6619. (b) Melinger, J. S.; Pan, Y.; Kleiman, V. D.; Peng, Z.; Davis, B. L.; McMorrow, D.; Lu, M. J. *Am. Chem. Soc.* **2002**, *124*, 12002. (c) Pan, Y.; Peng, Z.; Melinger, J. S. *Tetrahedron* **2003**, *59*, 5495. (d) Peng, Z.; Melinger, J. S.; Kleiman, V. *Photosynth. Res.* **2006**, *87*, 115.
- (8) (a) Xia, C. J.; Fan, X. W.; Locklin, J.; Advincula, R. C. *Org. Lett.* **2002**, *4*, 2067. (b) Xu, M. H.; Lin, J.; Hu, Q. S.; Pu, L. *J. Am. Chem. Soc.* **2002**, *124*, 14239. (c) Wang, J.; Luo, J.; Liu, L.; Zhou, Q.; Ma, Y.; Pei, J. *Org. Lett.* **2006**, *8*, 2281. (d) Nierengarten, J. *Pure Appl. Chem.* **2006**, *78*, 847. (e) Cotlet, M.; Vosch, T.; Habuchi, S.; Weil, T.; Muellen, K.; Hofkens, J.; De Schryver, F. *J. Am. Chem. Soc.* **2005**, *127*, 9760.
- (9) (a) Stewart, G. M.; Fox, M. A. *J. Am. Chem. Soc.* **1996**, *118*, 4354. (b) Balzani, V.; Campagna, S.; Denti, G.; Juris, A.; Serroni, S.; Venturi, M. *Acc. Chem. Res.* **1998**, *31*, 26. (c) Gilat, S. L.; Adronov, A.; Fréchet, J. M. J. *Angew. Chem., Int. Ed.* **1999**, *38*, 1422. (d) Dichtel, W. R.; Hecht, S.; Fréchet, J. M. J. *Org. Lett.* **2005**, *7*, 4451. (e) Hahn, U.; Gorka, M.; Vogtle, F.; Vicinelli, V.; Ceroni, P.; Maestri, M.; Balzani, V. *Angew. Chem., Int. Ed.* **2002**, *41*, 3595. (f) Kwon, T.-H.; Kim, M. K.; Kwon, J.; Shin, D.-Y.; Park, S.; Lee, C.-L.; Kim, J.-J.; Hong, J.-I. *Chem. Mater.* **2007**,

- 19, 3673. (g) Stewart, G. M.; Fox, M. A. *J. Am. Chem. Soc.* **1996**, *118*, 4354. (h) Vijayalakshmi, N.; Maitra, U. *Macromolecules* **2006**, *39*, 7931.
- (i) Adronov, A.; Gilat, S. L.; Frechet, J. M. J.; Ohta, K.; Neuwahl, F. V. R.; Fleming, G. R. *J. Am. Chem. Soc.* **2000**, *122*, 1175.
- (10) (a) Goodson, T., III *Annu. Rev. Phys. Chem.* **2005**, *56*, 581. (b) Poliakov, E. Y.; Chernyak, V.; Tretiak, S.; Mukamel, S. *J. Chem. Phys.* **1999**, *110*, 8161. (c) Shortreen, M. R.; Swallen, S. F.; Shi, Z. Y.; Tan, W.; Xu, Z.; Devadoss, C.; Moore, J. S.; Kopelman, R. *J. Phys. Chem. B* **1997**, *101*, 6318. (d) De Schryver, F. C.; Vosch, T.; Cotlet, M.; Auweraer, M. Van Der; Mullen, K.; Hofkens, J. *Acc. Chem. Res.* **2005**, *38*, 514. (e) Ahn, T. S.; Thompson, A. L.; Bharathi, P.; Muller, A.; Bardeen, C. J. *J. Phys. Chem. B* **2006**, *110*, 19810.
- (11) (a) Würthner, F. *Chem. Commun.* **2004**, 1564. (b) Weil, T.; Reuther, E.; Müllen, K. *Angew. Chem., Int. Ed.* **2002**, *41*, 1900. (c) Serin, J. M.; Brousmiche, D. W.; Fréchet, J. M. J. *Chem. Commun.* **2002**, 2605. (d) Sautter, A.; Kaletas, B. K.; Schmid, D. G.; Dobra, R.; Zimine, M.; Jung, G.; van Stokkum, I. H. M.; Cola, L. D.; Williams, R. M.; Würthner, F. *J. Am. Chem. Soc.* **2005**, *127*, 6719.
- (12) (a) Jones, B. A.; Ahrens, M. J.; Yoon, M. H.; Facchetti, A.; Marks, T. J.; Wasielewski, M. R. *Angew. Chem., Int. Ed.* **2004**, *43*, 6363. (b) Molinari, A. S.; Alves, H.; Chen, Z.; Facchetti, A.; Morpurgo, A. F. *J. Am. Chem. Soc.* **2009**, *131*, 2462. (c) An, Z.; Yu, J.; Jones, S. C.; Barlow, S.; Yoo, S.; Domercq, B.; Prins, P.; Siebbeles, L. D. A.; Kippelen, B.; Marder, S. R. *Adv. Mater.* **2005**, *17*, 2580.
- (13) Law, K. Y. *Chem. Rev.* **1993**, *93*, 449.
- (14) (a) Bao, Z.; Locklin, J., Eds. *Organic Field-Effect Transistors*; CRC Press: Boca Raton, FL, 2007. (b) Huttner, S.; Sommer, M.; Thelakkat, M. *Appl. Phys. Lett.* **2008**, *92*, 093302. (c) Struijk, C. W.; Sieval, A. B.; Dakhhorst, J. E. J.; van Dijk, M.; Kimkes, P.; Koehorst, R. B. M.; Donker, H.; Schaafsma, T. J.; Picken, S. J.; van de Craats, A. M.; Warman, J. M.; Zuilhof, H.; Sudholter, E. J. R. *J. Am. Chem. Soc.* **2000**, *122*, 11057. (d) Chesterfield, R. J.; McKeen, J. C.; Newman, C. R.; Ewbank, P. C.; da Silva, D. A.; Bredas, J. L.; Miller, L. L.; Mann, K. R.; Frisbie, C. D. *J. Phys. Chem. B* **2004**, *108*, 19281. (e) Oh, J. H.; Lee, H. W.; Mannsfeld, S.; Stoltenberg, R. M.; Jung, E.; Jin, Y. W.; Kim, J. M.; Yoo, J. B.; Bao, Z. N. *Proc. Natl. Acad. Sci. U.S.A.* **2009**, *106*, 6065. (f) Briseno, A. L.; Mannsfeld, S. C. B.; Reese, C.; Hancock, J. M.; Xiong, Y.; Jenekhe, S.; Bao, Z.; Xia, Y. *Nano Lett.* **2007**, *7*, 2847.
- (15) (a) Ranke, P.; Bleyl, I.; Simmerer, J.; Haarer, D.; Bacher, A.; Schmidt, H. W. *Appl. Phys. Lett.* **1997**, *71*, 1332. (b) Kalinowski, J.; Marco, P. D.; Fattori, V.; Giuletti, L.; Cocchi, M. *J. Appl. Phys.* **1998**, *83*, 4242. (c) Qu, J.; Zhang, J.; Grimsdale, A. C.; Müllen, K.; Jaiser, F.; Yang, X.; Neher, D. *Macromolecules* **2004**, *37*, 8297.
- (16) Zang, L.; Che, Y.; Moore, J. S. *Acc. Chem. Res.* **2008**, *41*, 1596.
- (17) (a) Tang, C. W. *Appl. Phys. Lett.* **1986**, *48*, 183. (b) Wohrle, D.; Krienenhoop, L.; Schnurpfeil, G.; Elbe, J.; Tennigkeit, B.; Hiller, S.; Schlettwein, D. *J. Mater. Chem.* **1995**, *5*, 1819. (c) Schmidt-Mende, L.; Fechtenkotter, A.; Mullen, K.; Moons, E.; Friend, R. H.; MacKenzie, J. D. *Science* **2001**, *293*, 1119. (d) Shin, W. S.; Jeong, H. H.; Kim, M. K.; Jin, S. H.; Kim, M. R.; Lee, J. K.; Lee, J. W.; Gal, Y. S. *J. Mater. Chem.* **2006**, *16*, 384. (e) Würthner, F.; Chen, Z. J.; Hoeben, F. J. M.; Osswald, P.; You, C. C.; Jonkheijm, P.; von Herrnhuyzen, J.; Schenning, A. P. H. J.; van der Schoot, P. P. A. M.; Meijer, E. W.; Beckers, E. H. A.; Meskers, S. C. J.; Janssen, R. A. J. *J. Am. Chem. Soc.* **2004**, *126*, 10611. (f) Zhan, X. W.; Tan, Z. A.; Domercq, B.; An, Z. S.; Zhang, X.; Barlow, S.; Li, Y. F.; Zhu, D. B.; Kippelen, B.; Marder, S. R. *J. Am. Chem. Soc.* **2007**, *129*, 7246.
- (18) Delgado, M. C. R.; Kim, E. G.; da Silva Filho, D. A.; Bredas, J. L. *J. Am. Chem. Soc.* **2010**, *132*, 3375.
- (19) Herrmann, A.; Weil, T.; Sinigersky, V.; Wiesler, U.-M.; Vosch, T.; Hofkens, J.; Schryver, F. C. D.; Müllen, K. *Chem.—Eur. J.* **2001**, *7*, 4844.
- (20) (a) Prathapan, S.; Yang, S. I.; Seth, J.; Miller, M. A.; Bocian, D. F.; Holten, D.; Lindsey, J. S. *J. Phys. Chem. B* **2001**, *105*, 8237. (b) Rytchinski, B.; Sinks, L. E.; Wasielewski, M. R. *J. Am. Chem. Soc.* **2004**, *126*, 12268. (c) Ego, C.; Marsitzky, D.; Becker, S.; Zhang, J.; Grimsdale, A. C.; Müllen, K.; MacKenzie, J. D.; Silva, C.; Friend, R. H. *J. Am. Chem. Soc.* **2003**, *125*, 437. (d) Loewe, R. S.; Tomizaki, K.-Y.; Youngblood, W. J.; Bo, Z.; Lindsey, J. S. *J. Mater. Chem.* **2002**, *12*, 3438. (e) Schlichting, P.; Duchscherer, B.; Seisenberger, G.; Basché, T.; Bräuchle, C.; Müllen, K. *Chem.—Eur. J.* **1999**, *5*, 2388. (f) Hinze, G.; Haase, M.; Nolde, F.; Müllen, K.; Basché, T. *J. Phys. Chem. A* **2005**, *109*, 6725.
- (21) (a) Sautter, A.; Kaletas, B. K.; Schmid, D. G.; Dobra, R.; Zimine, M.; Jung, G.; Van Stokkum, I. H. M.; De Cola, L.; Williams, R. M.; Würthner, F. *J. Am. Chem. Soc.* **2005**, *127*, 6719. (b) You, C.-C.; Hippus, C.; Grüne, M.; Würthner, F. *Chem.—Eur. J.* **2006**, *12*, 7510. (c) Stang, P. J.; Olenyuk, B. *Acc. Chem. Res.* **1997**, *30*, 502. (d) Würthner, F.; You, C.-C.; Saha-Möller, C. R. *Chem. Soc. Rev.* **2004**, *33*, 133. (e) Slone, R. V.; Benkstein, K. D.; Bélanger, S.; Hupp, J. T.; Guzei, I. A.; Rheingold, A. L. *Coord. Chem. Rev.* **1998**, *171*, 221. (e) Seidel, S. R.; Stang, P. J. *Acc. Chem. Res.* **2002**, *35*, 972.
- (22) (a) Würthner, F. *Topics in Current Chemistry*; Springer-Verlag: Berlin, 2005; Vol. 258. (b) Würthner, F.; Thalacker, C.; Sautter, A.; Schärfl, W.; Ibach, W.; Hollricher, O. *Chem.—Eur. J.* **2000**, *6*, 3871. (c) Peeters, E.; van Hal, P. A.; Meskers, S. C. J.; Janssen, R. A. J.; Meijer, E. W. *Chem.—Eur. J.* **2002**, *8*, 4470. (d) Würthner, F.; Chen, Z.; Dehm, V.; Stepanenko, V. *Chem. Commun* **2006**, *11*, 1188. (e) Hernandez, J.; de Witte, P. A. J.; van Dijk, E. M. H.; Kortrijk, J.; Nolte, R. J. M.; Rowan, A. E.; Garcia-Parajó, M. F.; Van Hulst, N. F. *Angew. Chem., Int. Ed.* **2004**, *43*, 4045. (e) Beckers, E. H. A.; Meskers, S. C. J.; Schenning, A. P. H. J.; Chen, Z.; Würthner, F.; Marsal, P.; Beljonne, D.; Cornil, J.; Janssen, R. A. J. *J. Am. Chem. Soc.* **2006**, *128*, 649. (f) Talukdar, P.; Bollot, G.; Mareda, J.; Sakai, N.; Matile, S. *J. Am. Chem. Soc.* **2005**, *127*, 6528. (g) Bhosale, S.; Sisson, A. L.; Talukdar, P.; Fürstenberg, A.; Banerji, N.; Vauthey, E.; Bollot, G.; Mareda, J.; Röger, C.; Würthner, F.; Sakai, N.; Matile, S. *Science* **2006**, *313*, 84.
- (23) (a) Pan, J.; Zhu, W.; Li, S.; Zeng, W.; Cao, Y.; Tian, H. *Polymer* **2005**, *46*, 7658. (b) Serin, J. M.; Brousmiche, D. W.; Frechet, J. M. J. *J. Am. Chem. Soc.* **2002**, *124*, 11848. (b) Augulis, R.; Pugzlys, A.; Hurenkamp, J. H.; Feringa, B. L.; van Esch, J. H.; van Loosdrecht, P. H. M. *J. Phys. Chem. A* **2007**, *111*, 12944. (c) Serin, J. M.; Brousmiche, D. W.; Fréchet, J. M. J. *Chem. Commun.* **2002**, 22, 2605.
- (24) (a) Schmaltz, B.; Weil, T.; Mullen, K. *Adv. Mater.* **2009**, *21*, 1067. (b) De Schryver, F. C.; Vosch, T.; Cotlet, M.; Van der Auweraer, M.; Muellen, K.; Hofkens, J. *Acc. Chem. Res.* **2005**, *38*, 514.
- (25) Qu, J.; Pschirer, N. G.; Liu, D.; Stefan, A.; De Schryver, F. C.; Mullen, K. *Chem.—Eur. J.* **2004**, *10*, 528.
- (26) Kohl, C.; Weil, T.; Qu, J.; Müllen, K. *Chem.—Eur. J.* **2004**, *10*, 5297.
- (27) Che, Y.; Yang, X.; Liu, G.; Yu, C.; Ji, H.; Zuo, J.; Zhao, J.; Zang, L. *J. Am. Chem. Soc.* **2010**, *132*, 5743.
- (28) (a) Chandrasekhar, S. *Liq. Cryst.* **1993**, *14*, 3. (b) Cross, S. J.; Goodby, J. W.; Hall, A. W.; Hird, M.; Kelly, S. M.; Toyne, K. J.; Wu, C. *Liq. Cryst.* **1998**, *25*, 1. (c) Boden, N.; Bushby, R. J.; Cammidge, A. N. *J. Am. Chem. Soc.* **1995**, *117*, 924.
- (29) Bagui, M.; Melinger, J.; Chakraborty, S.; Keightly, A. J.; Peng, Z. *Tetrahedron* **2009**, *65*, 1247.
- (30) Würthner, F.; Stepanenko, V.; Chen, Z.; Saha-Moeller, C. R.; Kocher, N.; Stalke, D. *J. Org. Chem.* **2004**, *69*, 7933.
- (31) Chen, Z.; Stepanenko, V.; Dehm, V.; Prins, P.; Siebbeles, L. D. A.; Seibt, J.; Marquetand, P.; Engel, V.; Würthner, F. *Chem.—Eur. J.* **2007**, *13*, 436.
- (32) (a) Baunsgaard, D.; Larsen, M.; Harrit, N.; Frederiksen, J.; Wilbrandt, R.; Stapelfeldt, H. *J. Chem. Soc., Faraday Trans.* **1997**, *93*, 1893. (b) Duzhko, V.; Shi, H.; Singer, K. D. *Langmuir* **2006**, *22*, 7947. (c) Marguet, S.; Markovitsi, D.; Millie, P.; Sigal, H.; Kumar, S. *J. Phys. Chem.* **1998**, *102*, 4697. (d) Markovitsi, D.; Germain, A.; Millie, P.; Lecuyer, P.; Gallos, L. K.; Argyrakis, P.; Bengs, H.; Ringsdorf, H. *J. Phys. Chem.* **1995**, *99*, 1005.
- (33) (a) Dubovskii, V. L.; Mikhal'chuk, A. L.; Raichenok, T. F.; Sobchuk, A. N.; Sukhodola, A. A.; Tolstorozhev, G. B. *J. Appl. Spectrosc.* **2006**, *73*, 347. (b) Lin, H.; Weng, Y.; Huang, H.; He, Q.; Zheng, M.; Bai, F. *Appl. Phys. Lett.* **2004**, *84*, 2980.
- (34) (a) Winnik, F. M. *Chem. Rev.* **1993**, *93*, 587. (b) Kim, H. J.; Hong, J.; Hong, A.; Ham, S.; Lee, J. H.; Kim, J. S. *Org. Lett.* **2008**, *10*, 1963.
- (35) Jones, B. A.; Facchetti, A.; Wasielewski, M. R.; Marks, T. J. *J. Am. Chem. Soc.* **2007**, *129*, 15259.

- (36) Förster, T. *Discuss. Faraday Soc.* **1959**, *27*, 7.
- (37) Paddon-Row, M. N. *Acc. Chem. Res.* **1994**, *27*, 18.
- (38) Weller, A. Z. *Phys. Chem. Neue Folge* **1982**, *133*, 93.
- (39) Molecular modeling shows that the bay position O to O distance is 7.51 Å and the N to N distance is 11.40 Å. Because the donor and PDI core are joined together by the bay position ether oxygen, the O–O distance was taken as the diameter of the anion. For G0, the distance from the center of the triphenylene core to ether O was taken as its ionic radii. For G1, the three triphenylene rings form a triangle. The distance from the center of this triangle to the ether O was taken as its ionic radii. The center-to-center distance  $R_{cc}$  is difficult to estimate as the donor G0 or G1 and the PDI core may fold to various extents. To simplify the calculation, the donor and the acceptor are assumed to be stretched out (no folding), in which case,  $R_{cc}$  is the sum of  $r^+$  and  $r^-$ .
- (40) (a) Gaines, G. L., III; O'Neil, M. P.; Svec, W. A.; Niemczyk, M. P.; Wasielewski, M. R. *J. Am. Chem. Soc.* **1991**, *113*, 719. (b) Neuteboom, E. E.; Beckers, E. H. A.; Meskers, S. C. J.; Meijer, E. W.; Janssen, R. A. J. *Org. Biomol. Chem.* **2003**, *1*, 198.
- (41) Oevering, H.; Paddon-Row, M. N.; Heppener, M.; Oliber, A. M.; Cotsaris, E.; Verhoeven, J. W.; Hush, N. S. *J. Am. Chem. Soc.* **1987**, *109*, 3258.
- (42) Zhong, H. Z.; Carlson, H. A. *Proteins: Struct., Funct., Bioinf.* **2005**, *58*, 222.
- (43) Case, D. A.; Darden, D. A.; Cheatham, T. E., III; Simmerling, C. L.; Wang, J.; Duke, R. E.; Luo, R.; Crowley, M.; Walker, R. C.; Zhang, W.; Merz, K. M.; Wang, B.; Hayik, S.; Roitberg, A.; Seabra, G.; Kolossvary, I.; Wong, K. F.; Paesani, F.; Vanicek, J.; Wu, X.; Brozell, S. R.; Steinbrecher, T.; Gohlke, H.; Yang, L.; Mongan, J.; Hornak, V.; Kollman, P. A. *AMBER10*, University of California, San Francisco, 2008.
- (44) Hornak, V.; Abel, R.; Okur, A.; Strockbine, B.; Roitberg, A.; Simmerling, C. L. *Proteins: Struct., Funct., Bioinf.* **2006**, *65*, 712.
- (45) Darden, T.; York, D.; Pedersen, L. *J. Chem. Phys.* **1993**, *98*, 10089.